JOURNAL OF GEOPHYSICAL RESEARCH, VOL. 111, C11011, doi:10.1029/2006JC003497, 2006

Transient wind-driven upwelling in a submarine canyon: A process-oriented modeling study

Jochen Kämpf[1]

Received 20 January 2006; revised 26 June 2006; accepted 20 July 2006; published 22 November 2006.

[1] A hydrodynamic model is employed to study flow near a submarine canyon during conditions of upwelling-favorable coastal winds. Findings reveal that up-canyon flow is the rapid geostrophic adjustment to barotropic pressure gradients establishing across the canyon. Stratification leads to the formation of a cyclonic eddy within the canyon, trapping neutrally buoyant matter, and limits the upwelling depth only when a strong seasonal pycnocline is located below shelf-break depth. Typical speeds of up-canyon flow are 10–30 cm/s. Constrained by the timescale of synoptic weather patterns (~5 days), only stronger events (high upwelling index) can move slope water from a depth >300 m onto the continental shelf and close toward the coast, where it can be lifted into surface layers during a subsequent upwelling event.

Citation: Kämpf, J. (2006), Transient wind-driven upwelling in a submarine canyon: A process-oriented modeling study, *J. Geophys. Res.*, *111*, C11011, doi:10.1029/2006JC003497.

1. Introduction

[2] Submarine canyons cutting across the shelf break are bathymetric features found along many continental margins. Their typical width is 10–50 km, depth variations across canyons are 100–500 m, and cross-canyon topographic slopes can be as steep as 45°. In the presence of upwelling-favorable winds, observational evidence taken from the Astoria Canyon (north-western coast of North America) suggests that submarine canyons locally enhance the upwelling of subsurface water onto the continental shelf [*Hickey*, 1997; *Allen et al.*, 2001; *Mirshak and Allen*, 2005]. Upwelled water comes typically from a depth of 300 m. Greater source depths of 400 m have been reported for the Juan de Fuca Canyon in the North West Pacific Ocean [*Freeland and Denman*, 1982]. Several field studies [*Kinsella et al.*, 1987; *Hickey*, 1997; *Signorini et al.*, 1997] have shown that, during a stronger upwelling event, the flux across the shelf break through a canyon is 1 order of magnitude larger that in the bottom Ekman layer on the adjacent continental slope. Dynamical mechanisms inherent with this flow enhancement are still poorly understood. Moreover, during stronger upwelling events, upwelling prevails throughout the canyon, while a cyclone is found within the canyon [*Hickey*, 1997].

[3] *Mirshak and Allen* [2005] summarize the present-day, still incomplete understanding of the dynamics of flow through a canyon during upwelling-favorable conditions. This is briefly described in the following. Overall, canyon upwelling requires a geostrophic shelf-break current with a direction opposite of Kelvin wave propagation. In a stratified system, near-surface currents are not markedly affected by the canyon but deeper currents are altered by it. The analytical considerations of *Freeland and Denman* [1982] suggest that some of the flow will turn into the canyon, where geostrophic currents are blocked by canyon walls, producing an unbalanced cross-shelf pressure gradient that drives flow up the canyon. As water at shelf-break depth flows over the canyon rim, it descends into the canyon. This descent leads to vortex-tube stretching [e.g., *Hickey*, 1997], which results in the addition of cyclonic vorticity and turns the flow up the canyon. Some of the up-canyon flow will be upwelled onto the continental shelf. Deeper in the canyon, the currents steered up the canyon cause the isopycnals to tilt, balancing the barotropic pressure gradient [*Allen*, 1996]. This process is sometimes referred to as buoyancy shutdown [e.g., *Chapman*, 2002]. It should be noted that the analytical model of the force balance across a canyon by Freeland and Denman (pp. 1087, 1982) neglects the Coriolis force under the assumption that the canyon is "narrow"; that is, the Rossby number on length scales of the canyon width is assumed to be large compared with unity. The latter assumption, however, does generally not hold, given that Canyon Rossby numbers, even for narrow canyons <10 km in width, can be estimated of the order of 0.1–0.5 [e.g., *Mirshak and Allen*, 2005]. This indicates a substantial influence of the Coriolis force on the length scale of typical canyon widths, being neglected in the dynamical model by *Freeland and Denman* [1982].

[4] Numerical models have been employed to explore the general nature of canyon flow, but various sources of truncation errors (in terrain-following models) are believed to lead to difficulties in replicating the flow field seen in laboratory studies [*Allen et al.*, 2003; *Boyer et al.*, 2004]. Nevertheless, numerical findings have generally aided in the interpretation of field data.

[1]School of Chemistry, Physics and Earth Sciences, Flinders Research Centre for Coast and Catchment Environments, Flinders University, Adelaide, South Australia, Australia.

0148-0227/06/2006JC003497$09.00

[5] *Klinck* [1996] employed a semispectral primitive equation model (SPEM) to study the circulation near a submarine canyon. The rigid-lid model was forced by prescription of coastal sea level via boundary conditions for the barotropic stream function. This created an alongshore flow of ~10 cm/s in speed. For unknown reasons, vertical friction was excluded. Findings indicate that canyon upwelling develops for a shelf-break current flowing in a direction opposite to Kelvin wave propagation, which occurs for upwelling-favorable coastal wind. The downwelling case in *Klinck* [1996], on the other hand, showed no pronounced disturbances near the canyon. Instead of this, the flow appeared to be almost perfectly topographically steered along bathymetric contours of the canyon. *Klinck* [1996] concluded that the direction of alongshore flow near the canyon controls the canyon effect, whereas density stratification determines the vertical distance over which the canyon affects the alongshore flow. It is noticeable that *Klinck* [1996] used a fairly long spin-up time of the model forcing of 10 days, so that responses to synoptic wind variation was not described. Also effects of variations of the speed of the incident alongshore flow on canyon upwelling dynamics were not studied.

[6] *Ardhuin et al.* [1999] employed a three-dimensional, free-surface regional coastal ocean model with a vertical z-coordinate (vertical grid spacing was 50 m) in their study of the circulation in a steep canyon off the Catalan coast (western Mediterranean). In contrast to the studies of *Klinck* [1996], the model domain included a quasi-realistic irregular coastline and bathymetry that under certain wind conditions showed a marked remote influence on the circulation over the nearby canyon.

[7] *She and Klinck* [2000] employed the Rutgers University Ocean Model (ROMS), based on a modified terrain-following coordinate (s-coordinate), to study canyon-flow interactions under constant wind-stress forcing applied over 15 days. They conclude that steady canyon-flows establish on timescales of ~5 days and that a closed circulation is established within the canyon in response to vortex stretching (upwelling) or compression (downwelling). These results differed from previous findings of *Klinck* [1996] in that the circulation forced by downwelling winds was largely opposite to that forced by upwelling winds. Effects of wind strength on canyon-flow interaction were not studied.

[8] On the basis of laboratory studies in conjunction with interpretation of previous field observations from the Astoria Canyon, *Mirshak and Allen* [2005] suggested that the strength of incident shelf-break flow controls the upwelling flux in a canyon. According to their studies, the upwelling flux is in proportion to $U^{8/3}$, where U is the speed of the incident alongslope flow, so that exclusively swifter (>10 cm/s) alongslope flow triggers noticeable canyon upwelling.

[9] Canyon-upwelling of subsurface nutrient-enriched water generally supports highly productive and highly diverse marine food webs [e.g., *Bosley et al.*, 2004]. Under certain circumstances, however, recurrent upwelling events of nutrients can lead to depletion of dissolved oxygen and detrimental effects on the marine ecosystem [*Figley et al.*, 1979; *Glenn et al.*, 1996]. The theoretical model of *Song et al.* [2001] indicates that alongshore-varying topography, such as introduced by submarine canyons, controls the formation of such devastating upwelling centers.

[10] *Song and Chao* [2004] developed an analytical model in their study of topographic effects on coastal upwelling. Nevertheless, this model excludes a key process inherent with the upwelling process; namely, bottom friction, and uses a rigid lid which eliminates barotropic flow. Therefore, the solutions discussed by *Song and Chao* [2004] describe only limited aspects of the upwelling process.

[11] The general aim of this work to improve the theoretical understanding of canyon-flow interaction during upwelling-favorable winds. Specific objectives are to examine whether significant canyon upwelling can occur on synoptic timescales (~5 days), to address dynamical mechanisms inherent with this upwelling, to address factors that control the depth of upwelling, and to quantify the upwelling response to different forcing scenarios and ambient conditions (strength of ambient alongslope flow, density stratification, topographic details). To this end, a state-of-the-art three-dimensional hydrodynamic model, described below, is applied in a process-oriented mode under a variety of forcing and initial conditions.

[12] The South Australian Coastal Upwelling System [*Kämpf et al.*, 2004] is chosen as the reference observational framework for this study. This wind-driven upwelling system typically experiences 2–3 major upwelling events during austral (December–April) summer, seen as individual upwelling centers along the Bonney Coast, off the south-western coast of Kangaroo Island, and along the southern tip of Eyre Peninsula (Figure 1). Interestingly, upwelling among these centers often responds in unison and almost instantaneously to coastal wind forcing, which is puzzling given that the continental shelf in the eastern Great Australian Bight (which supports high abundance of pilchards, southern bluefin tuna, and many other marine species) is much wider (~100 km) compared with that along the Bonney Coast (~20 km). The author postulates that submarine canyons cutting across the shelf break south of Kangaroo Island (Figure 2), in particular the de Couedic Canyon, trigger localized subsurface upwelling of slope water onto the shelf fertilizing the eastern Great Australian Bight.

[13] This paper is organized as follows. Section 2 describes the numerical model employed in the work and details the experimental design. Section 3 presents and discusses results. Section 4 summarizes the key findings of this study and makes suggestions for future research.

2. Methods

2.1. Model Description

[14] This paper employs a barotropic-baroclinic model that couples the three-dimensional, hydrodynamic High-Resolution Bottom-Boundary Layer model (HiReBBL), developed and described by *Kämpf* [2000] and *Kämpf and Fohrmann* [2000], with a barotropic shallow-water-equation model. *Kämpf* [2005] used this coupled model to study the descent of dense water near a submarine canyon at high latitudes. A brief description of this model is given in the following.

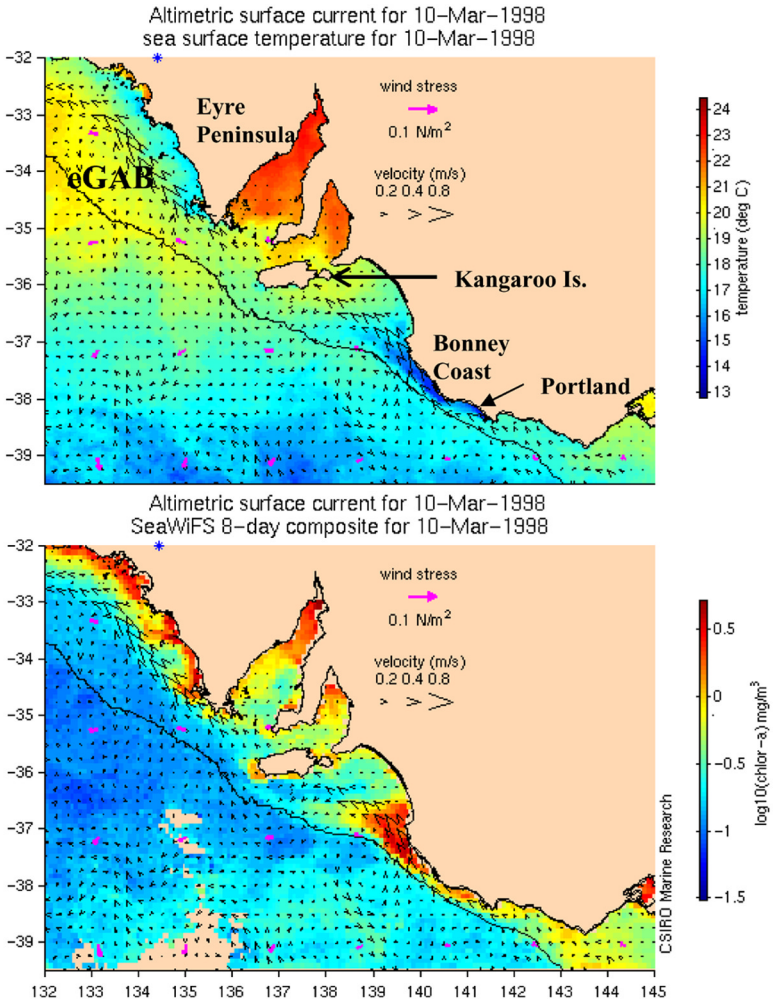

Figure 1. Satellite-derived distributions of (top) sea surface temperature (°C) and (bottom) surface chlorophyll-a (logarithmic scale) during a major coastal upwelling event, 10 March 1998. The solid line shows the 200-m topographic contour, representing the shelf break. The eastern Great Australian Bight is denoted as eGAB. Adapted from *Kämpf et al.* [2004].

[15] A two-dimensional shallow-water-equation model is used to capture barotropic currents driven by sea-level gradients. Horizontal momentum equations of this model are given by

$$\frac{\partial U}{\partial t} + U\frac{\partial U}{\partial x} + V\frac{\partial U}{\partial y} - fV = -g\frac{\partial \eta}{\partial x}, \tag{1a}$$

$$\frac{\partial V}{\partial t} + U\frac{\partial V}{\partial x} + V\frac{\partial V}{\partial y} + fU = -g\frac{\partial \eta}{\partial y}, \tag{1b}$$

where (x, y) are Cartesian horizontal coordinates, t is time, (U, V) is horizontal velocity, $f = -0.9 \times 10^{-4}$ s^{-1} is the Coriolis parameter (considering the South Australian continental shelf), $g = 9.81$ m s^{-2} is acceleration due to gravity, and η is sea-surface elevation. The vertically integrated form of the continuity equation is given by

$$\frac{\partial \eta}{\partial t} + \frac{\partial}{\partial x}[(H - h^*)U] + \frac{\partial}{\partial y}[(H - h^*)V] + \frac{\partial}{\partial x}(h^*\langle u\rangle) + \frac{\partial}{\partial y}(h^*\langle v\rangle) = 0, \tag{2}$$

where $H(t, x, y) = H_o(x, y) + \eta(t, x, y)$ is the total water depth with H_o being the undisturbed depth, h^* is the constant vertical extension of a bottom-following layer modeled by HiReBBL (see below) with vertically averaged horizontal flow components $\langle u\rangle$ and $\langle v\rangle$.

[16] HiReBBL consists of a bottom-following ocean layer of constant thickness h^* that is resolved by constant vertical grid spacing. The governing equations are cast in a rotated, bottom-following coordinate system, being similar to sigma coordinates [see *Kämpf*, 2000]. The design of this model allows for tracing of thin, bottom-arrested, variable-density flows over highly variable bottom topography without a loss in vertical resolution. Similar to other terrain following coordinate model, this model is subject to truncation errors owing to a rotation of the vertical coordinate and curvature of bottom-parallel coordinate surfaces. These errors, however, are reasonably small for greatly smoothed bottom topography and mild bottom slopes as is the case in my experiments where the maximum bottom slope is <4°.

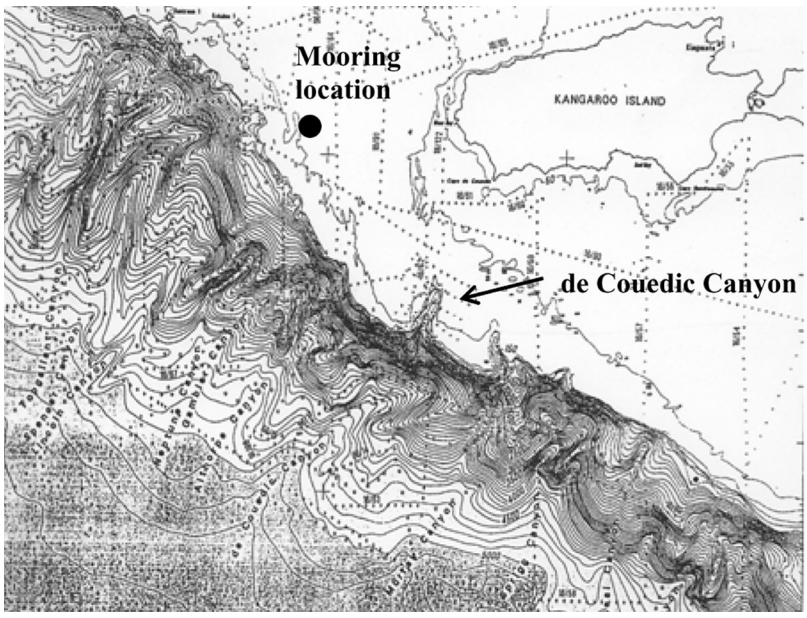

Figure 2. Bathymetry south of Kangaroo Island. Contour interval is 100 m for water depths >300 m and 50 m otherwise. Courtesy of Australian Geological Survey Organisation, Canberra, Australia. The solid circle indicates the location of a bottom mooring measuring lateral velocity with a recording interval of 15 min over the period June 1982–May 1983. CTD data have been acquired at this location (sampling interval 1–2 months) during the period November 1980–June 1983.

[17] Horizontal coordinates (x, y) are Cartesian ones and a bottom-following vertical coordinate z^* is introduced by

$$z^* = z + H_o - h^*, \tag{3}$$

where z is the conventional vertical Cartesian coordinate, and $H_o(x, y)$ is the undisturbed total water depth (sea-level variations are ignored). Thus, the model subdomain employed for HiReBBL ranges from $z^* = -h^*$ at the seafloor to $z^* = 0$ at its surface. After conversion to z^* coordinates, conservation equations for momentum and volume in the bottom-following subdomain can be written as [*Kämpf*, 2000]

$$\frac{\partial u}{\partial t} + Adv(u) - fv = -\frac{1}{\rho_o}\frac{\partial P}{\partial x} + \frac{\partial H_o}{\partial x}g' + Diff(u), \tag{4a}$$

$$\frac{\partial v}{\partial t} + Adv(v) + fu = -\frac{1}{\rho_o}\frac{\partial P}{\partial y} + \frac{\partial H_o}{\partial y}g' + Diff(v), \tag{4b}$$

$$\frac{\partial w^*}{\partial t} + Adv(w^*) = -\frac{1}{\rho_o}\frac{\partial P}{\partial z^*} - \gamma g' + Diff(w^*), \tag{4c}$$

$$\frac{\partial u}{\partial x} + \frac{\partial v}{\partial y} + \frac{\partial w^*}{\partial z^*} = 0, \tag{4d}$$

where $Adv(.)$ and $Diff(.)$ denote advection and diffusion operators, P is dynamic pressure, $\rho_o = 1028$ kg m^{-3} is reference density, $g' = \rho'/\rho_o$ g is reduced gravity with ρ' being a density anomaly, w^* is vertical velocity, and $\gamma^2 = 1 - (\partial H_o/\partial x)^2 - (\partial H_o/\partial y)^2$. The use of bottom-following coordinates splits the lateral pressure-gradient force into two parts: a pressure-gradient force parallel to the sea floor and "buoyant-slope" terms that describe acceleration of a dense fluid on a sloping seafloor. Evolution of the density field is predicted from

$$\frac{\partial \rho'}{\partial t} + Adv(\rho') = Diff(\rho'). \tag{5}$$

The advection operator is given by

$$Adv(\psi) = u\frac{\partial \psi}{\partial x} + v\frac{\partial \psi}{\partial y} + w^*\frac{\partial \psi}{\partial z^*}. \tag{6}$$

Turbulent diffusion is formulated according to [*Mellor and Blumberg*, 1985]

$$Diff(\psi) = \frac{\partial}{\partial x}\left(A_h\frac{\partial \psi}{\partial x}\right) + \frac{\partial}{\partial y}\left(A_h\frac{\partial \psi}{\partial y}\right) + \frac{\partial}{\partial z^*}\left(A_v\frac{\partial \psi}{\partial z^*}\right). \tag{7}$$

For simplicity, eddy diffusivity is assumed to be equal to eddy viscosity. Horizontal (bottom-parallel) eddy viscosity is formulated by the Smagorinsky formula [*Oey et al.*, 1985]; that is,

$$A_h = c_h^2 \Delta x \Delta y\, t_h^{-1}, \tag{8}$$

where Δx and Δy are horizontal grid spacings, the parameter c is set to 0.4 and the turbulent timescale is given by $t_h^{-2} = (\partial u/\partial x)^2 + (\partial v/\partial y)^2 + 0.5(\partial u/\partial y + \partial v/\partial x)^2$. Vertical eddy viscosity is parameterized by means of [*Kochergin*, 1987]

$$A_v = (c_v \Delta z)^2 t_v^{-1}, \tag{9}$$

where Δz is vertical grid spacing, the parameter c_v is set to 0.15 and the turbulent timescale is determined from $t_v^{-2} = (\partial u/\partial z)^2 + (\partial v/\partial z)^2 - N^2$, where the stability frequency is $N^2 = -g/\rho_o \partial \rho'/\partial z$. Background vertical viscosity is set to 10^{-5} m^2/s. Bottom friction is described by a conventional quadratic law with a bottom drag coefficient chosen as

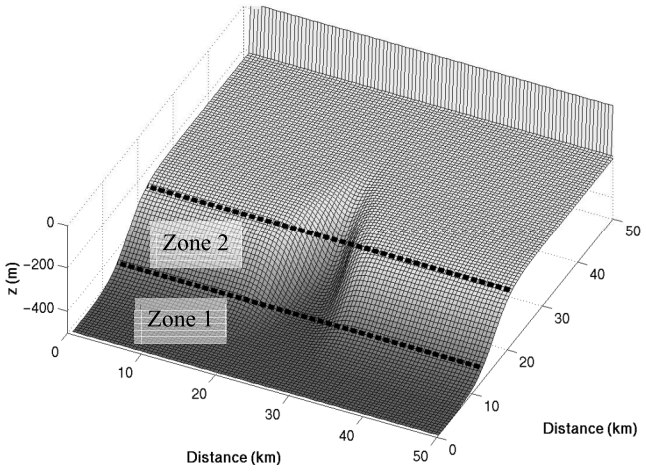

Figure 3. Topographic contours (m) of model bathymetry. Lateral grid spacing is 500 m. Two zones are selected for analysis of passive tracer trajectories.

r = 0.003. Results, presented below, are qualitatively not sensitive to parameter choices in the turbulence closures. Flow of information from the barotropic model to HiReBBL is realized by dynamic boundary conditions in terms of continuity in dynamic pressure; that is, $P = \rho_o g\eta$ at z* = 0. Moreover, horizontal viscous stresses are assumed to vanish at z* = 0, which implies that horizontal flow is depth-independent across the z* = 0 interface. Note that this pressure condition implies that HiReBBL simultaneously simulates barotropic and baroclinic modes. Mode splitting is not employed. *Kämpf* [2000] and *Kämpf and Fohrmann* [2000] describe the numerical solver of (4a)–(4d). The barotropic model uses an explicit Eulerian-forward time stepping algorithm and an upstream advection scheme. Moreover, the trajectories of nonbuoyant particles are predicted from a simple three-dimensional advection algorithm. Diffusive effects on tracer trajectories can be ignored on timescales (∼5 days) considered in this paper.

2.2. Experimental Design

[18] A series of numerical experiments has been conducted considering variations in forcing conditions, density stratification and bottom topography. Figure 3 displays the idealized bottom topography employed for the experiments. This bathymetry is analogue to that used by *Klinck* [1996]. The x-axis is aligned parallel to the shelf break and the y-axis is perpendicular to the coast. Total water depth varies from 220 m on the shelf to 500 m in the deepest parts of the model domain. The northern boundary constitutes a land boundary (coast). The submarine canyon has a width of ∼10 km. The maximum depth variation across the canyon is ∼150 m. The maximum bottom inclination introduced across the canyon is ∼4°. Canyon-induced depth variations vanish both near the coast and in the deepest part of the model domain, the latter to avoid dynamical disturbances at the open-ocean boundary. Horizontal grid spacing is set to 500 m, resolving the canyon width by 20 grid points. The subdomain of HiReBBL has a vertical extension of h^* = 220 m, resolved by a vertical grid spacing of 10 m. This implies that the subdomain of HiReBBL extends to the sea surface on the continental shelf, which allows for full coastal upwelling along the coast without truncation of baroclinic pressure gradients. Limitations of the model are instances in which denser water is locally upwelled past the vertical extent of the bottom layer. This, however, does not occur in the present study within simulation times of a few days.

[19] Instead of employing wind-stress forcing (yielding similar results), the model is forced by the prescription of coastal sea level with uniform value along the coast. This has been motivated by sea-level observations from Portland (Bonney Coast) that show a direct response of sea level to upwelling index (Figure 4). From this data, it is evident that

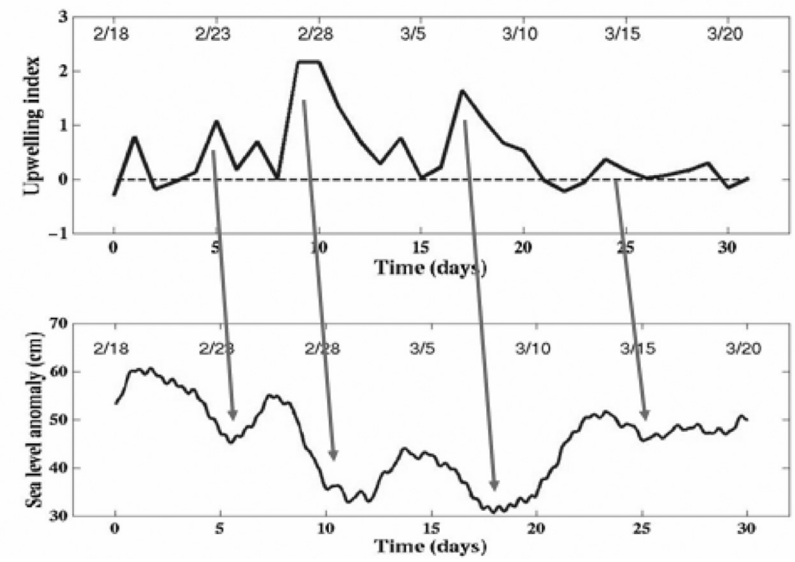

Figure 4. Time series of (top) upwelling index (arbitrary units) and sea-level anomaly (cm) for the Bonney Coast (Portland), 18 February–30 March 1998. Tides are removed from sea-level data. Atmospheric data were provided by Bureau of Meteorology (BoM, Australia). Sea-level data are courtesy of National Tidal Centre (NTC, Australia).

Table 1. Summary of Numerical Experiments

Experiment	Coastal Sea Level Anomaly, cm	N^2 Below 320 m, 10^{-5} s^{-2}	Comments
1	−10	0.954	Reference experiment
2a	−5	0.954	Reduced coastal upwelling
2b	−15	0.954	Enhanced coastal upwelling
3a	−10	0.477	Weaker density stratification
3b	−10	1.431	Enhanced density stratification
3c	−10	0.954	Density jump (0.5 kg/m^3) at 320-m depth
4	−10	0	No stratification
5	+10	0.954	Downwelling case with stratification
6	−10	-	Shallow seasonal pycnocline; see Appendix A

upwelling events are characterized by coastal sea-level drops of the order of 5–15 cm on synoptic timescales of ~5 days. In the model, the prescribed coastal sea-level anomaly is linearly adjusted from zero to its final value over the initial 2 days of simulation and then held constant for another 3 days. Initially the ocean is at rest. The time step chosen is 2 s, being limited by the Courant-Friedrich-Levy (CFL) stability criterion for the barotropic wave mode. The sea level at the southern, open-ocean boundary is always kept at its initial value. Zero-gradient conditions are used along western and eastern boundaries. Vertical density stratification is included, but the model limitation is that this has to be confined to the terrain-following subdomain of HiReBBL. Accordingly, for the bathymetric configuration used, density variations had to be confined to water depths deeper than 300 m. Two different zones are used for analysis of passive tracer trajectories (see Figure 3). To this end, 1000 tracers are initially distributed randomly in space in the lowermost 50 m of the water column in each of these zones. Tracers leaving the model domain through one lateral boundary are reintroduced through the opposite boundary.

[20] Table 1 summarizes numerical experiments discussed in this paper. Experiment 1, chosen as a reference run, considers a coastal sea-level drop of 10 cm. It includes linear density stratification commencing below a water depth of 320 m. On the basis of field observations off the shelf break south of Kangaroo Island [*Hahn*, 1986], a vertical density change of 0.1 kg/m^3 per 100 m is chosen, corresponding to $N^2 = 9.5 \times 10^{-6}$ s^{-2}. In Experiments 2a–b, the sea-level drop is varied to values of 5 cm and 15 cm, respectively, to examine effects owing to a variation in coastal upwelling intensity. Experiments 3a–c consider variations in density stratification. In Exp. 3a the vertical density change is halved to 0.05 kg/m^3 per 100 m, whereas a stronger stratification of 0.15 kg/m^3 per 100 m is assumed in Exp. 3b. Exp. 3c includes a strong density jump of 0.5 kg/m^3 at a depth horizon of 320 m to investigate whether the existence of a relatively deep seasonal pycnocline alters the upwelling dynamics. In addition to this, Appendix A discusses the case of canyon upwelling in presence of a shallow pycnocline situated well above shelf-break depth. This experiment is not included in the main text body as it considers a topographic configuration different to the other model runs. Exp. 4 considers a coastal sea-level drop of 10 cm with a water column void of stratification, whereas Exp. 5 investigates a downwelling scenario using a temporary coastal sea-level rise of 10 cm. The aim of this is to explore asymmetries between the upwelling and downwelling cases.

3. Results and Discussion

3.1. Upwelling Scenarios With Stratification (Reference Experiment)

[21] Figure 5a displays the upper-ocean flow field together with sea-level anomalies after 5 days. The prescribed

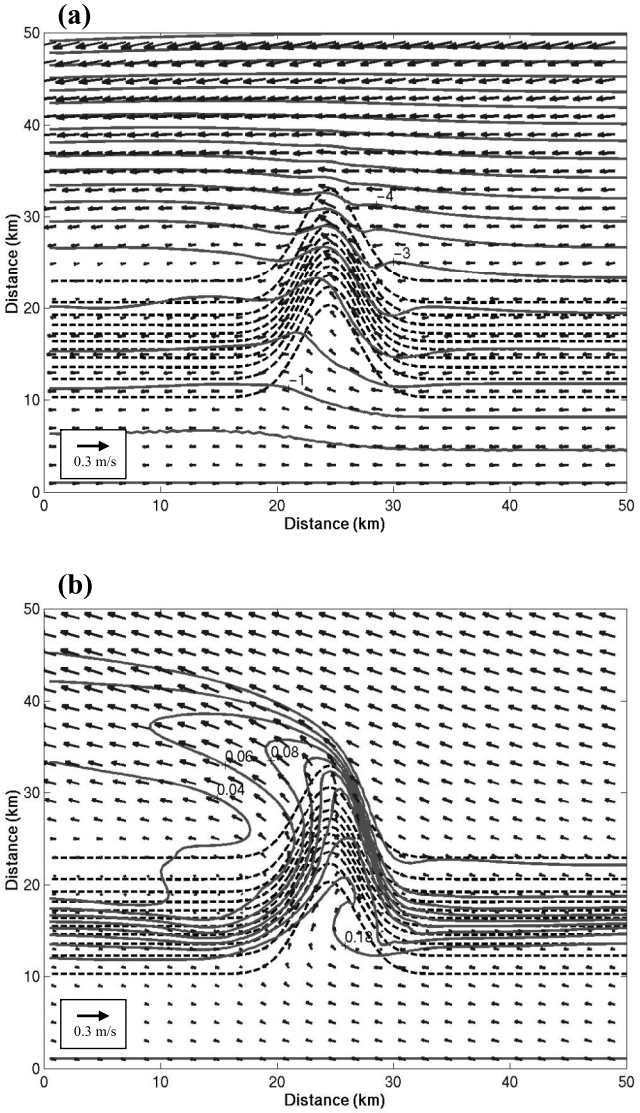

Figure 5. Exp. 1. Results after 5 days of simulation. (a) Sea-level contours (solid lines, CI = 0.5 cm) and upper-ocean horizontal flow vectors (arrows). (b) Contours of near-bottom density anomalies (solid lines, CI = 0.02 kg m^{-3}) and near-bottom flow vectors (arrows). Dashed lines are topographic contours (CI = 25 m). Flow vectors are averaged over 4 × 4 grid cells for visualization purposes. "Near-bottom" refers to the lowest grid point of HiReBBL which is located 5 m above the seafloor.

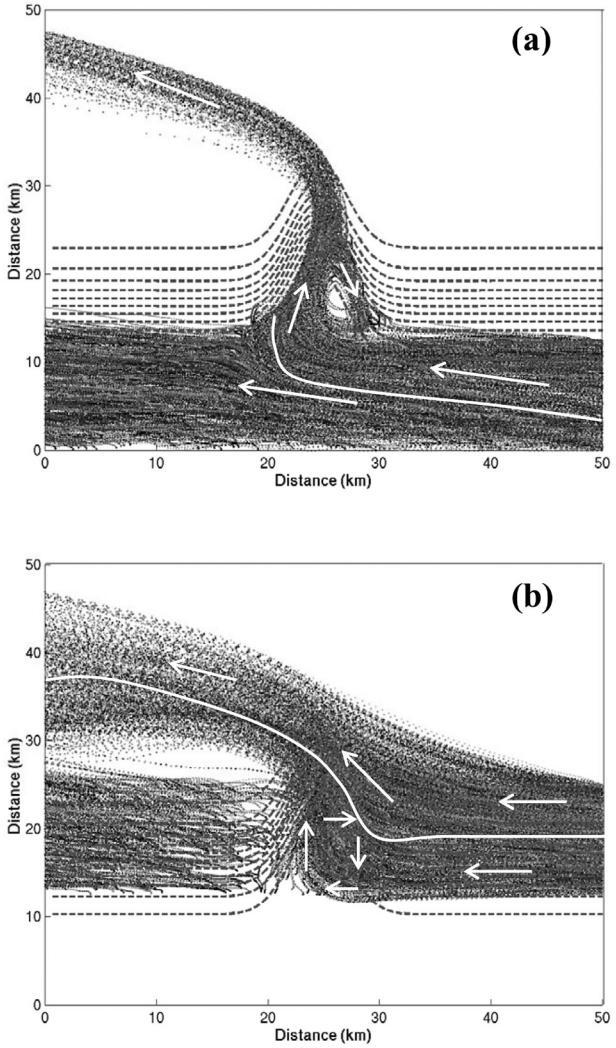

Figure 6. Exp. 1. Trajectories of passive tracers initially released in the lowermost 50 m of the water column in (a) zone 1 and (b) zone 2 over 5 days of simulation. See Figure 3 for definition of zones. Dashed lines are topographic contours (CI = 25 m). Arrows indicate the flow direction.

coastal sea-level drop of 10 cm creates a swift (∼30 cm/s) coastal upwelling jet being right-bounded by the coast. Along the continental slope there is a zone of diminished flow speeds of ∼10 cm/s. The surface flow is largely in geostrophic balance; that is, running along sea-level contours. Canyon topography operates to distort the ambient geostrophic flow field. Resultant sea-level variations across the canyon are <1 cm, which cannot be detected by means of satellite altimetry, and the upper-ocean flow is relatively undisturbed except in close vicinity of the canyon axis. A high-pressure anomaly appears to start at the canyon axis and weakens downstream aiming to barotropically steer the incident flow along topographic contours in a geostrophic fashion. Instead of this, topographic steering remains incomplete and weak upper-ocean onshore flow establishes in most parts of the canyon. The Canyon Rossby Number, comparing inertia effects with rotational effects on length scales of the canyon width, is ∼0.15 is this experiment, suggesting that rotational effects are dominant while inertia effects cannot fully be ignored.

[22] On the shelf, the near-bottom flow (Figure 5b) attains an onshore ageostrophic flow component owing to frictional effects in the bottom Ekman layer, ∼10–20 m in thickness. The near-bottom flow is steered up the entire length of the canyon at a speed of ∼14 cm/s. Initially, on the downstream side of the canyon, the incident barotropic flow moves denser water up the canyon sidewalls. The resultant baroclinic pressure gradient intensifies across-canyon pressure gradients in the bottom-boundary layer and operates to geostrophically steer deeper water up the canyon. In upper parts on the upstream side of the canyon, on the other hand, inertia effects lead to the formation of a narrow density front. This front extends onto the shelf and is associated with a swift geostrophic frontal jet that moves deeper slope water onto the shelf. Once on the shelf, in turn, buoyant-slope effects become weaker and onshore density gradients across this front can sustain an alongshore jet. As a combination of geostrophic adjustment processes taking place at both sides of the canyon, upwelling occurs in most parts of canyon, in agreement with observational evidence [*Hickey*, 1997], and triggers a channeled flow of denser slope water from water depths of up to 500 m onto the continental shelf and close toward the shore (Figure 6).

[23] A cyclonic eddy forms in deeper parts of the canyon owing to disturbances in the density field. This eddy separates the upwelling flow into two distinct branches (see Figure 6). A deeper branch of the upwelling flow is located at water depths of 300–500 m. It carries deeper slope water toward the canyon where it becomes topographically steered up the canyon. However, some of this flow merges with the cyclonic eddy that operates as a trap for neutrally buoyant particles, whereas other portions of the flow escape onto the continental shelf. The second branch of upwelling flow is located on the upper continental slope in a depth range of 200–300 m. This shallower flow does not become entrained by the cyclonic eddy but experiences a pronounced onshore displacement of ∼20 km while trying to move past the canyon. On the continental shelf, these two branches of the upwelling circulation eventually merge and continue to travel along the coast by means of the overall alongshore drift. Farther downstream, this water mass might be lifted into surface layers during the course of a subsequent upwelling-favorable wind event. The continental slope downstream the canyon is void of upwelling features. This is associated with substantial weakening of near-bottom flow owing to buoyancy shutdown [see *Chapman*, 2002]; that is, a compensation of barotropic pressure gradients into baroclinic pressure gradients (see also Figure 5b). Consequently, a continental margin void of submarine canyons would suppress wind-induced upwelling in a stratified ocean. Note that buoyancy shutdown requires lateral pressure gradients in the bottom layer to be opposed to that in the upper ocean. This does not occur in the canyon itself, where cross-canyon baroclinic pressure gradients in the bottom layer (on the downstream side of the canyon) rather intensify the barotropic pressure gradient established across the canyon (see Figure 5).

[24] Flow along the shelf is geostrophically driven by onshore pressure gradients and modified by bottom friction

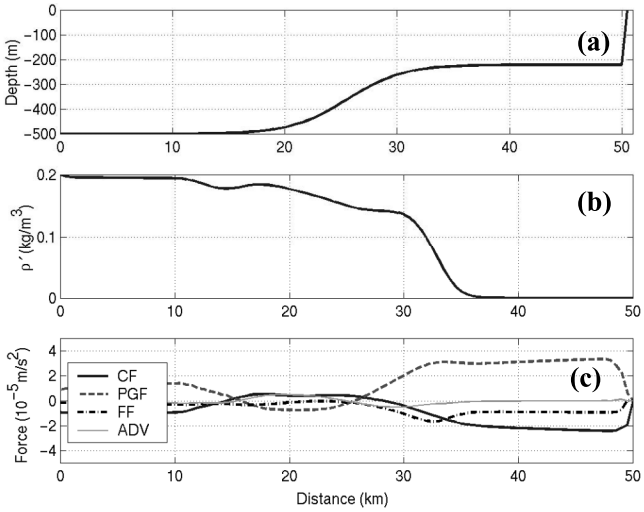

Figure 7. Exp. 1. Distributions along x = 25 km of (a) bathymetry, (b) near-bottom density anomaly, and (c) near-bottom y-components of forces (per unit mass) at day 5. CF, Coriolis force; PGF, pressure gradient force; FF, friction force; ADV, nonlinear terms. "Near-bottom" refers to the lowest grid point of HiReBBL which is located 5 m above the seafloor.

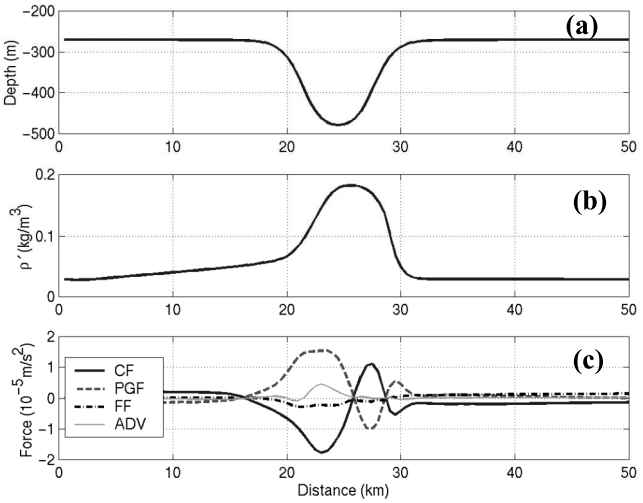

Figure 8. Exp. 1. Distributions along y = 20 km cutting across the canyon of (a) bathymetry, (b) near-bottom density anomaly, and (c) near-bottom x-components of forces (per unit mass) at day 5. CF, Coriolis force; PGF, pressure gradient force; FF, friction force; ADV, nonlinear terms. "Near-bottom" refers to the lowest grid point of HiReBBL which is located 5 m above the seafloor.

(Figure 7) that induces onshore flow in the bottom Ekman layer. Across the density front of the upwelling water on the upper continental slope, the onshore pressure gradient dramatically weakens owing to buoyancy shutdown and so does the along-shelf flow. Farther down in the canyon, the pressure gradient even reverses its direction. This component of the pressure gradient force therefore cannot drive water up the canyon, which contradicts previous suggestions made by *Freeland and Denman* [1982].

[25] On the other hand, the up-canyon flow is largely in geostrophic balance with cross-canyon pressure gradients (Figure 8). As a result of this, a swift geostrophic up-canyon flow establishes along the downstream side of the canyon. Down-canyon flow, being part of the anticyclonic eddy, establishes on the other side of the canyon. Frictional and nonlinear effects play only an insignificant role in the dynamics. Thus, the canyon upwelling process can be interpreted as a rapid geostrophic response to pressure gradients establishing across a canyon during upwelling-favorable coastal winds. This has been articulated before [*Klinck*, 1988, 1989]. Note that a steady-state force balance is reached within only a few inertia periods (1–2 days).

[26] For stronger coastal sea-level drops of ~15 cm (Exp. 2b), the resultant canyon upwelling is relatively deep with the deepest upwelled water stemming from a depth of 500 m and the cyclonic eddy in the canyon largely disappears (not shown). For a moderate sea-level drop of 5 cm (Exp. 2a), the resultant upwelling is only shallow (<350 m) and deeper slope water becomes trapped in a well-developed cyclonic eddy (not shown). This indicates that stronger coastal upwelling events lead to deeper upwelling in a canyon.

3.2. Effects of Stratification

[27] Moderate variation in the strength of the subsurface stratification (Exp. 3a–b), however, has only little impact of the resultant canyon upwelling (not shown). Only the extreme case of a deep and strong pycnocline located below shelf-break depth (Exp. 3c) stops the upwelling of water from below this depth onto the shelf. Instead of this, a strong cyclonic eddy establishes over the canyon (Figure 9) and only few particles trapped in this eddy are eventually released onto the continental shelf (Figure 10). Nevertheless, shallow canyon upwelling still occurs but is limited to the water column above pycnocline depth. Note that this depth-restriction of canyon upwelling, also found by *Klinck*

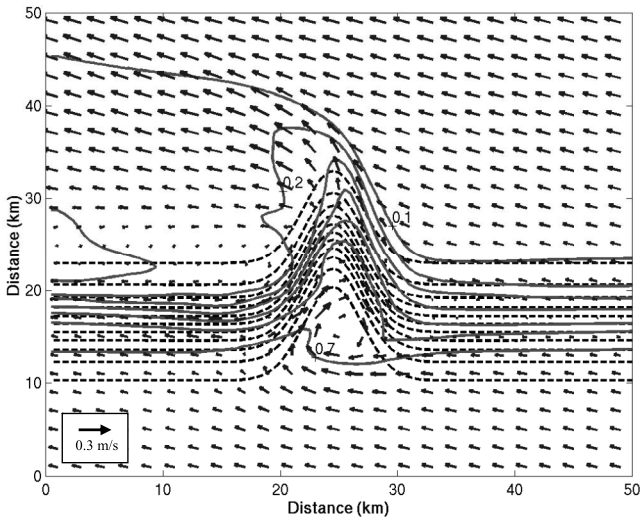

Figure 9. Exp. 3c. Results after 5 days of simulation. Contours of near-bottom density anomalies (solid lines, CI = 0.1 kg m^{-3}) and near-bottom flow vectors (arrows). Flow vectors are averaged over 4 × 4 grid cells for visualization purposes. Dashed lines are topographic contours (CI = 25 m). "Near-bottom" refers to the lowest grid point of HiReBBL which is located 5 m above the seafloor.

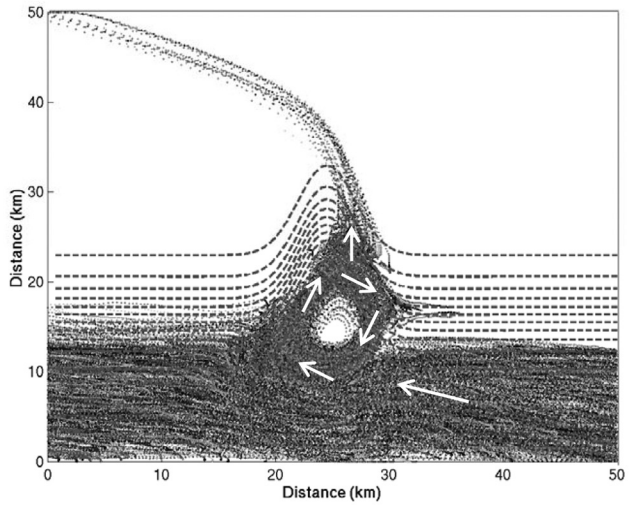

Figure 10. Exp. 3c. Results after 5 days of simulation. Trajectories of passive tracers initially released in the lowermost 50 m of the water column in zone 1 over 5 days of simulation. See Figure 3 for definition of zones. Dashed lines are topographic contours (CI = 25 m). Arrows indicate the flow direction.

[1996], requires a fairly deep seasonal pycnocline that intersects the continental slope below shelf-break depth. Such situations might only be encountered during convective mixed-layer deepening in winter. This depth restriction is absent in experiments considering a shallow (50–150 m) summertime pycnocline that is located well above shelf-break depth (see Appendix A).

3.3. Upwelling Scenario Without Stratification

[28] In Exp. 4, void of stratification, the prescribed coastal sea-level drop of 10 cm creates a swift (~30 cm/s) coastal upwelling jet being right-bounded by the coast. Off the shelf break, speeds of this westward flow diminish to ~15 cm/s (Figure 11). The surface flow is largely geostrophically balanced, whereas the bottom flow attains an onshore ageostrophic flow component owing to frictional effects in the bottom Ekman layer. Canyon-flow interaction interaction creates sea-level variations across the canyon of ~2 cm. Geostrophic, largely depth-independent upwelling flow establishes in most parts of the canyon. This result disagrees with *Ardhuin et al.* [1999], who stated that density stratification is essential for models to reproduce cross-isobath flows over canyons. Interestingly, in contrast to the shelf currents, the up-canyon flow, described here, is almost barotropic, which is only possible bacause nonlinear terms (advection of momentum) compensate for frictional effects in this region (not shown). The author deems this as one of the curious cases in which barotropic geostrophic flow can cross topographic contours, but, indeed, the flow is not strictly geostrophic as it contains frictional and advective processes that, however, tend to cancel out each other. Note that eddy formation is absent in this experiment.

3.4. Upwelling Versus Downwelling

[29] A transient coastal sea-level rise, associated with downwelling favorable winds, yields a left-bounded along-slope flow (southern hemisphere) opposite to that for the upwelling case (Figure 12). In interaction with the submarine canyon, a low-pressure anomaly establishes over the canyon aiming to steer the flow along topographic contours. The fundamental difference between this situation and that governing the upwelling case is the existence of an ambient barotropic pressure gradient directed offshore. This gradient supports flow with a down-canyon component in favor of that with an up-canyon component (owing to direction-dependant compensation of frictional effects), so that an

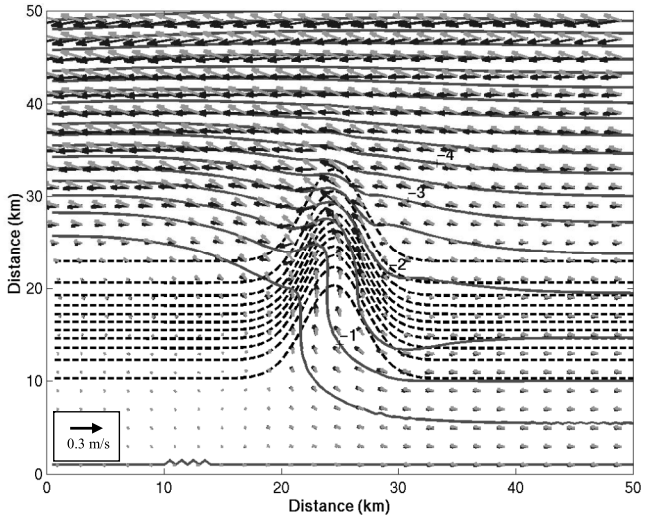

Figure 11. Exp. 4. Sea-level contours (solid lines, CI = 0.5 cm), upper-ocean horizontal flow (black arrows) and near-bottom flow (gray arrows) after 5 days of simulation. Flow vectors are averaged over 4 × 4 grid cells for visualization purposes. Dashed lines are topographic contours (CI = 25 m). "Near-bottom" refers to the lowest grid point of HiReBBL which is located 5 m above the seafloor.

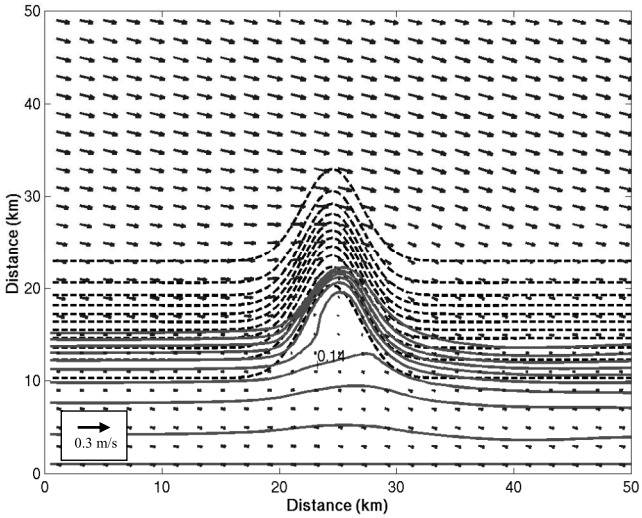

Figure 12. Exp. 5. Results after 5 days of simulation. Contours of near-bottom density anomaly (solid lines, CI = 0.02 kg m^{-3}) and near-bottom flow vectors (arrows). Flow vectors are averaged over 4 × 4 grid cells for visualization purposes. Dashed lines are topographic contours (CI = 25 m). "Near-bottom" refers to the lowest grid point of HiReBBL which is located 5 m above the seafloor.

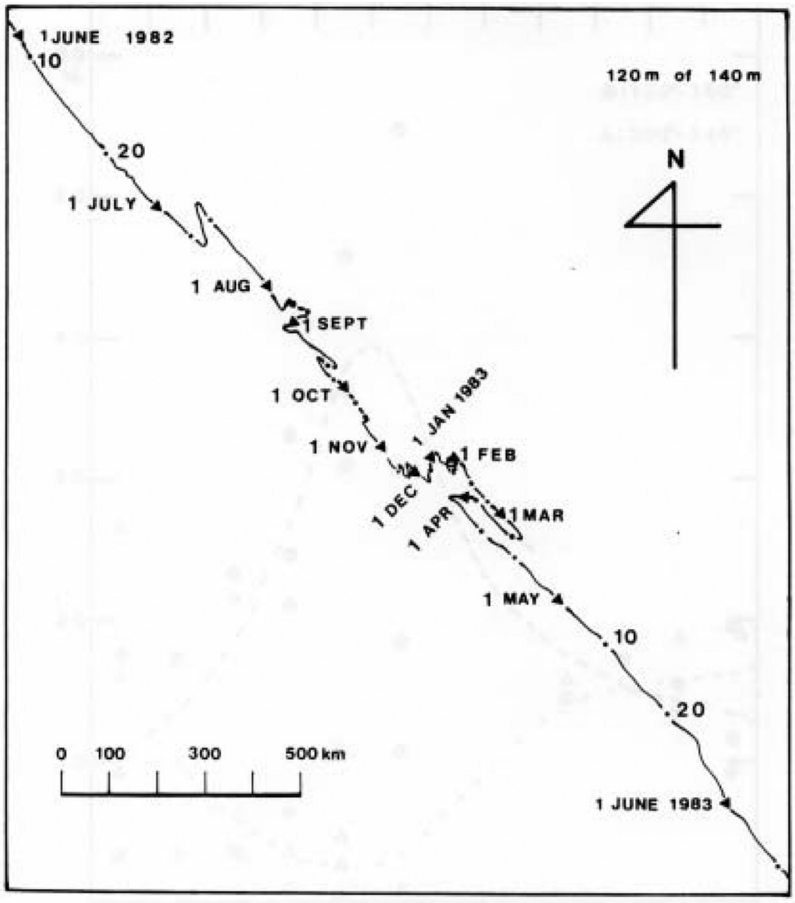

Figure 13. Progressive vector diagram of near-bottom velocity (14-day averages) at the mooring location shown in Figure 2. From *Hahn* [1986].

overall downward displacement occurs as the flow moves past the canyon. In a stratified ocean, this downward displacement leads to a disturbance in the density field such that the resultant baroclinic pressure gradients in bottom layers compensate barotropic pressure gradients. This effect (buoyancy shutdown) leads to the disappearance of flow at some depth below the shelf break (see Figure 12). Note that, in contrast to the upwelling case, this buoyancy shutdown also takes place inside the canyon, where baroclinic pressure gradients in the bottom layer (across the canyon) oppose barotropic cross-canyon pressure gradients formed in the upper ocean (not shown). Also note that a mesoscale eddy is not created in Exp. 5.

3.5. Observational Evidence

[30] Mooring data taken near the shelf break southwest of Kangaroo Island (see Figure 2) show a general southeastward drift at speeds of 10–20 cm/s (Figure 13). This flow, which is a signature of the South Australian Current [e.g., *Kämpf et al.*, 2004], does not support upwelling for it travels in the direction of Kelvin wave propagation [e.g., *Klinck*, 1996]. During austral summer (December–April), however, the flow reverses its direction in several episodes during which it flows transiently toward the northwest with speeds of 10–15 cm/s. These episodes correspond to upwelling of colder water across the shelf break (Figure 14) and can be interpreted as wind-driven upwelling events [*Kämpf et al.*, 2004]. Note that the event occurring in March 1983 is pronounced with strong signals seen in both the bottom flow reversal and the temperature data. This suggests that episodes of northwestward flow seen in the data are the signature of localized canyon upwelling events that induce a northwestward flow along the shelf (see Figure 6). The author postulates that it is a series of such flow events that the bottom mooring has recorded. Moreover, summer data from the Climatology of Australian Regional Seas (CARS) reveal a pool of cold bottom water located southwest to west of Kangaroo Island (see Figure 3 in *McClatchie et al.* [2006]). This pool appears to have its source in vicinity of the de Couedic canyon. This is further evidence of the integral effect of a series of localized canyon-upwelling events.

4. Summary and Conclusions

[31] This paper considers the interaction of alongslope flow with a submarine canyon during upwelling-favorable winds on synoptic timescales (<5 days). Findings are in general agreement with observational evidence and capture the key features of the canyon-upwelling process. On the basis of model results some unresolved issues in canyon dynamics could be resolved.

[32] Substantial deep canyon upwelling can occur within timescales <5 days. This upwelling is the more intensive the

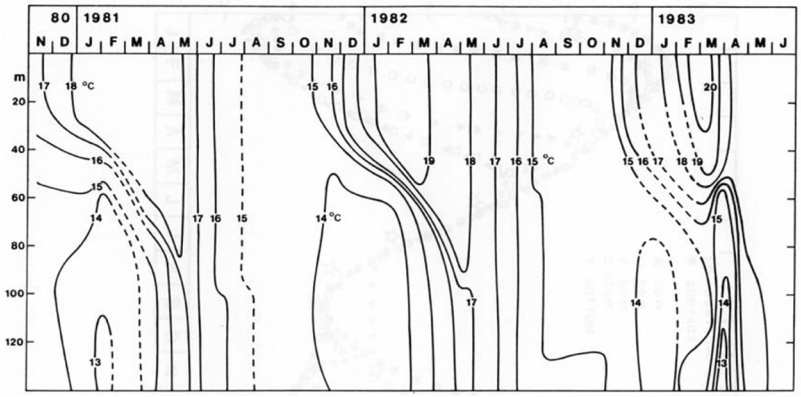

Figure 14. Time series of vertical temperature profiles (sampling interval ~1–2 months) at the mooring location shown in Figure 2. From *Hahn* [1986].

stronger the coastal wind event (greater upwelling index). This is in agreement with numerical results of *She and Klinck* [2000]. My findings suggest that up-canyon flow is the rapid geostrophic adjustment to barotropic pressure gradients establishing across a canyon and not, as previously suggested [e.g., *Freeland and Denman*, 1982], by ageostrophic flow driven by a cross-shelf pressure gradient. Indeed the latter is vanishingly small deeper in the canyon (or even reverses the direction), so that the flow becomes subtle to cross-canyon pressure gradients.

[33] Disturbances in the density field operate to enhance the canyon-upwelling process, but are not essential in the generation thereof. The major effect of stratification appears to be the formation of a cyclonic eddy within the canyon that operates as a trap for neutrally buoyant matter. In the case of a strong density stratification below shelf-break depth (deep winter pycnocline), this eddy blocks up-canyon flows and only shallow upwelling from a depth 200–300 m can occur. On the other hand, strong upwelling-favorable wind events (high upwelling index) lead to disappearance of this eddy and support a much deeper upwelling from below 400 m.

[34] The speed of up-canyon flow increases with the strength of the coastal wind event. A steady-state canyon circulation establishes relatively rapid (within 2 days), but owing to advective delay and limited time it is only the strongest events, associated with sea-level drops >10 cm, that move deeper slope water onto the continental shelf. The deepness of the upwelling circulation is therefore mainly controlled by strength and duration of upwelling-favorable wind conditions (sometimes referred to as "wind impulse" [see *Cushman-Roisin*, 1994]) and, for a deep seasonal pycnocline located below shelf-break depth, by stratification.

[35] During strong upwelling-favorable coastal wind events, submarine canyons "pump" deeper slope water onto the shelf where it flows along the coast along with the general wind-induced shelf current. This water remains confined to bottom layers, in support of subsurface primary production, and might be brought toward the surface during the course of a subsequent wind event. Thus, it appears that localized canyon-upwelling events can fertilize large areas on the adjacent continental shelf. This study suggests that a particular submarine canyon situated south of Kangaroo Island, the de Couedic Canyon, does this for a large portion of the eastern Great Australian Bight.

[36] The model used in this study had the limitation that density stratification was confined to the vertical extent of the bottom-following subdomain. This also limited the maximum depth of the continental slope under investigation. Other suitable models, such as generalized s-coordinate models [e.g., *Haidvogel et al.*, 1991] adopted with a uniform vertical grid spacing in the bottom boundary layer, might be applied in the future to explore the canyon-upwelling dynamics for a greater variety of ambient conditions.

[37] Future research on the canyon-upwelling process should explore how the net upwelling flux varies for different forcing conditions and canyon configurations, as an extension to previous laboratory spin-up experiments of *Mirshak and Allen* [2005]. This might lead to improved empirical bulk formula of cross-shelf fluxes inherent with up-canyon flow for manifold use in multidisciplinary upwelling studies. More observational campaigns are required to improve understanding of the fate and biological implications of locally upwelled water along the continental shelf.

Appendix A: Canyon Upwelling in the Presence of a Shallow Seasonal Pycnocline

[38] An additional experiment has been performed to examine whether the existence of a shallow seasonal pycnocline (thermocline) above shelf-break depth influences or even stops the canyon upwelling process. For this purpose, a modified topography is used in which total water depth is limited to 340 m, so that the top surface of the HiReBBL domain approaches a depth horizon of 140 m in the deepest parts of the model domain. A strong initial density jump of 1 kg m^{-3} is prescribed at a depth level of 160 m (shelf-break depth is 220 m). Below this density jump, density is assumed to increase linearly with depth at a rate of 0.1 kg/m^3 per 100 m. A sea-level drop of 10 cm is prescribed along the coast as in Exp. 1.

[39] The overall effect of a shallow pycnocline in the upper ocean is to weaken the alongshore flow on the continental shelf (Figure A1, compare with Figure 5b). This effect, reducing the speed of the alongshore flow by 50–80%, is associated with a baroclinic compensation of

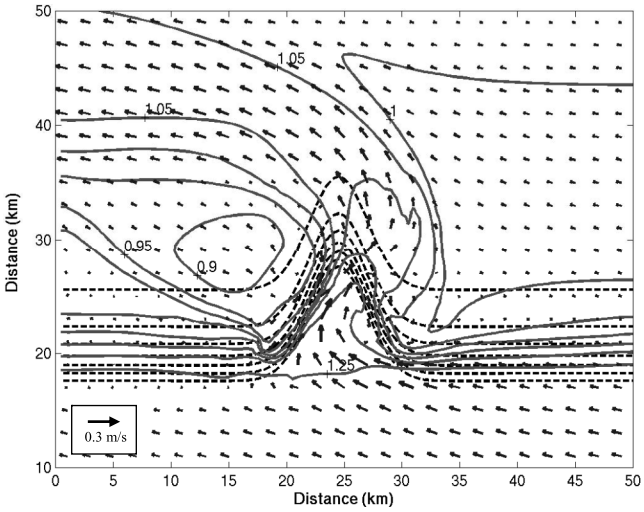

Figure A1. Exp. 6. Results after 5 days of simulation. Contours of near-bottom density anomaly (solid lines, CI = 0.05 kg m^{-3}) and near-bottom flow vectors (arrows) at day 5. Flow vectors are averaged over 4 × 4 grid cells for visualization purposes. Dashed lines are topographic contours (CI = 17 m). "Near-bottom" refers to the lowest grid point of HiReBBL which is located 5 m above the seafloor.

the on-shore pressure gradient in surface layers by opposite baroclinic pressure gradients in bottom layers created by upward displacement of the pycnocline. Note that this adjustment does not lead to a full buoyancy shutdown in this simulation. More importantly is that the existence upper-ocean stratification has not much influence on the canyon-upwelling process itself. In other word, this experiment demonstrates that up-canyon flow is not significantly affected by density stratification in the upper ocean and the deepest water (from 340 m in the experiment) becomes injected onto the shelf during the 5 days of simulation. Findings suggest that only strong stratification below shelf-break depth can limit the canyon upwelling process as in Exp. 3c. Overall, this suggests that the existence of a shallow thermocline (pycnocline) in summer does not hinder the canyon upwelling process.

[40] **Acknowledgments.** I thank the South Australian Partnership of Advanced Computing (SAPAC) for the use of their facilities. This research was supported by various smaller research grants from Flinders University, Australia.

References

Allen, S. E. (1996), Topographically generated, subinertial flows within a finite length canyon, *J. Phys. Oceanogr.*, *26*, 1608–1632.

Allen, S. E., C. Vindeirinho, R. E. Thomson, M. G. Foreman, and D. L. Mackas (2001), Physical and biological processes over a submarine canyon during an upwelling event, *Can. J. Fish. Aquat. Sci.*, *58*, 671–684.

Allen, S. E., M. S. Dinniman, J. M. Klinck, D. D. Gorby, A. J. Hewett, and B. M. Hickey (2003), On vertical advection truncation errors in terrain-following numerical models: Comparison to a laboratory model for upwelling over submarine canyons, *J. Geophys. Res.*, *108*(C1), 3003, doi:10.1029/2001JC000978.

Ardhuin, F., J.-M. Pinot, and J. Tintoré (1999), Numerical study of the circulation in a stepp canyon off the Catalan coast (western Mediterranean), *J. Geophys. Res.*, *104*(C5), 11,115–11,135.

Bosley, K. L., J. W. Lavelle, R. D. Brodeur, W. W. Wakefield, R. L. Emmett, E. T. Baker, and K. M. Rehmke (2004), Biological and physical processes in and around Astoria submarine Canyon, Oregon, USA, *J. Mar. Syst.*, *50*, 21–37.

Boyer, D. L., D. B. Haidvogel, and N. Pérenne (2004), Laboratory-numerical model comparisons of canyon flows: A parameter study, *J. Phys. Oceanogr.*, *34*, 1588–1609.

Chapman, D. C. (2002), Deceleration of a finite-width, stratified current over a sloping bottom: Frictional spindown or buoyancy shutdown?, *J. Phys. Oceanogr.*, *32*, 336–352.

Cushman-Roisin, B. (1994), *Introduction to Geophysical Fluid Dynamics*, 320 pp., Prentice-Hall, Upper Saddle River, N. J.

Figley, W. B., B. Pyle, and B. Halgren (1979), Oxygen depletion and associated benthic mortalities in New York Bight, 1976: Sociaeconomic impacts, edited by R. L. Swanson and C. J. Sindermann, *NOAA Prof. Pap. 11*, Natl. Oceanic and Atmos. Admin., Silver Spring, Md.

Freeland, H., and K. Denman (1982), A topographically controlled upwelling centre off Vancouver Island, *J. Mar. Res.*, *40*, 1069–1093.

Glenn, S., M. Crowley, D. Haidvogel, and Y. T. Song (1996), Underwater observatory captures coastal upwelling events off New Jersey, *Eos Trans. AGU*, *77*, 233–236.

Hahn, S. D. (1986), Physical structure of the waters of the South Australian continental shelf, Ph.D. thesis, 284 pp., Flinders Univ. of South Aust., Adelaide, Australia.

Haidvogel, D. B., J. L. Wilkin, and R. E. Young (1991), A semi-spectral primitive equation ocean circulation model using vertical sigma and orthogonal curvilinear horizontal coordinates, *J. Comput. Phys.*, *94*, 151–185.

Hickey, B. M. (1997), The response of a steep-sided, narrow canyon to time-variable wind forcing, *J. Phys. Oceanogr.*, *27*, 697–726.

Kämpf, J. (2000), Impact of multiple submarine channels on the descent of dense water at high latitudes, *J. Geophys. Res.*, *105*, 8753–8773.

Kämpf, J. (2005), Cascading-driven upwelling in submarine canyons at high latitudes, *J. Geophys. Res.*, *110*, C02007, doi:10.1029/2004JC002554.

Kämpf, J., and H. Fohrmann (2000), Sediment-driven downslope flow in submarine canyons and channels: Three-dimensional numerical experiments, *J. Phys. Oceanogr.*, *30*(9), 2302–2319.

Kämpf, J., M. Doubell, D. Griffin, R. L. Matthews, and T. M. Ward (2004), Evidence of a large seasonal coastal upwelling system along the Southern Shelf of Australia, *Geophys. Res. Lett.*, *31*, L09310, doi:10.1029/2003GL019221.

Kinsella, E. D., A. E. Hay, and W. W. Denner (1987), Wind and topographic effects on the Labrador current at Carson canyon, *J. Geophys. Res.*, *92*, 10,853–10,869.

Klinck, J. (1988), The influence of a narrow transverse canyon on initially geostrophic flow, *J. Geophys. Res.*, *93*, 509–515.

Klinck, J. (1989), Geostrophic adjustment over submarine canyons, *J. Geophys. Res.*, *94*, 6133–6144.

Klinck, J. (1996), Circulation near submarine canyons: A modeling study, *J. Geophys. Res.*, *101*, 1211–1223.

Kochergin, V. P. (1987), Three-dimensional prognostic models, in *Three-Dimensional Coastal Ocean Models*, *Coastal Estuarine Stud.*, vol. 4, edited by N. S. Heaps, pp. 201–208, AGU, Washington, D. C.

McClatchie, S., J. F. Middleton, and T. M. Ward (2006), Water mass analysis and alongshore variation in upwelling intensity in the eastern Great Australian Bight, *J. Geophys. Res.*, *111*, C08007, doi:10.1029/2004JC002699.

Mellor, G. L., and A. F. Blumberg (1985), Modeling vertical and horizontal diffusivities with the sigma coordinate system, *Mon. Weather Rev.*, *113*, 1380–1383.

Mirshak, R., and S. E. Allen (2005), Spin-up and the effects of a submarine canyon: Application to upwelling in Astoria Canyon, *J. Geophys. Res.*, *110*, C02013, doi:10.1029/2004JC002578.

Oey, L.-Y., G. L. Mellor, and R. I. Hires (1985), A three-dimensional simulation of the Hudson-Raritan estuary. 1: Description of the model and model simulation, *J. Phys. Oceanogr.*, *15*, 1676–1692.

She, J., and J. Klinck (2000), Flow near submarine canyons driven by constant winds, *J. Geophys. Res.*, *105*, 28,671–28,694.

Signorini, S. R., A. Münchow, and D. Haidvogel (1997), Flow dynamics of a wide Arctic canyon, *J. Geophys. Res.*, *102*, 18,661–18,680.

Song, Y. T., and Y. Chao (2004), A theoretical study of topographic effects on coastal upwelling and cross-shore exchange, *Ocean Modell.*, *6*, 151–176.

Song, Y. T., D. B. Haidvogel, and S. M. Glenn (2001), Effects of topographic variability on the formation of upwelling centers off New Jersey: A theoretical model, *J. Geophys. Res.*, *106*(C5), 9223–9240.

J. Kämpf, School of Chemistry, Physics and Earth Sciences, Flinders Research Centre for Coast and Catchment Environments, Flinders University, Adelaide, SA 5001, Australia. (jochen.kaempf@flinders.edu.au)